THE JOURNAL OF PHYSICAL CHEMISTRY C

pubs.acs.org/JPCC Article

Multicolor Chemical Imaging by Sum Frequency Generation Imaging Microscopy of Monolayers on Metal Surfaces

Aleksandr A. Pikalov, Tianlang Yu, Daniela Rodriguez, Han Ju Lee, T. Randall Lee, and Steven Baldelli*

Cite This: J. Phys. Chem. C 2020, 124, 16908−16917 Read Online

ACCESS | Metrics & More | Article Recommendations | Supporting Information

ABSTRACT: Sum frequency generation imaging microscopy (SFG-IM) is a unique surface-specific technique that can detect the spatial distributions of differing monolayer species based on chemical contrast. Here SFG images of microcontact-patterned multicomponent self-assembled monolayers derived by the adsorption of alkanethiols on gold were analyzed by factor analysis (FA) utilizing a library consisting of SFG alkanethiol spectra to determine the chemical identity and spatial distribution of the patterned monolayers across the images. By utilizing the spectral library as a target test for factor analysis, we correctly identified the monolayer species, and their spatial distributions were mapped. The chemical identity and spatial distribution of a random-pattern multicomponent alkanethiol sample were determined and mapped. Furthermore, utilizing the alkanethiol library, factor analysis was able to identify an unknown monolayer region, the vibrational spectra of which were not present in the target library. The results demonstrate the capability of FA combined with the spectral library to determine the chemical composition and spatial distribution of organic molecules on the surface of multicomponent complex chemical systems acquired by SFG-IM.

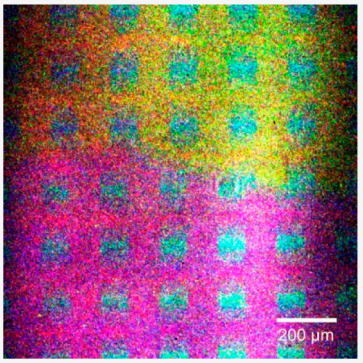

INTRODUCTION

The ability to detect the spatial distribution of distinct molecular species on the surface is essential for gaining a fundamental understanding of complex chemical systems. While there are many different optical imaging systems, the majority lack surface sensitivity, and many rely on fluorescent or vibrational probes or other secondary methods to generate image contrast. Sum frequency generation imaging microscopy (SFG-IM) is a unique surface-specific technique for obtaining the spatial distribution of molecules with label-free chemical contrast on surfaces.[1−3] The capability of submonolayer sensitivity allows investigation of spatially inhomogeneous systems to map chemical surface distribution, molecular arrangement, orientation, and domain formation.[4−7] The technique provides information regarding the interfacial structure of a surface, such as molecular coverage, molecular orientation, chemical reactions, and molecular adsorption.[2,8−13] Sum frequency generation microscopy has been used to study a range of systems such as monolayers on metals, nonlinear materials, and biological systems.[3,7,14−17] However, these systems typically contain at most two species that are assumed to be homogeneously distributed.

Vibrational spectroscopic imaging techniques including Fourier-transform infrared, Raman, coherent anti-Stokes Raman, and stimulated Raman scattering can provide spatial structures and chemical information about the molecules present on the surface.[18−26] The limitation of these techniques, as surface microscopy tools, is that they lack interface specificity and cannot distinguish the surface from the bulk signal. The advantage of SFG is its intrinsic sensitivity to molecules in a noncentrosymmetric environment, where inversion symmetry is broken;[6,27,28] this feature makes analysis by the SFG process highly surface specific.

Detailed information about the surface molecular spatial distribution, molecular arrangement, orientation, and domain formation obtained by SFG-IM have been acquired through spectral fitting.[3,7,14,15,29−32] However, SFG has been mainly limited to binary chemical systems, since at any single wavelength only two chemical species can be distinguished, and spectral fitting is limited to the spectral resolution of chemical species, signal-to-noise ratio, and spectral congestion.[8,29,30,33−38] A few SFG studies have utilized spectral decomposition to generate chemical maps.[35,37]

Chemometrics and analytical techniques, such as partial least-squares, principal component analysis, multivariate analysis, and factor analysis, have been utilized in spectral and image analysis in many spectroscopic techniques.[39−47] Factor analysis (FA) is a statistical method that uses mathematical procedures to investigate whether some observed variables are linearly related to some smaller number of unobservable factors. The application of FA in chemistry has been pioneered by Malinowski in the 1980s.[39] The FA method

Received: March 7, 2020
Revised: July 9, 2020
Published: July 22, 2020

https://dx.doi.org/10.1021/acs.jpcc.0c02038
J. Phys. Chem. C 2020, 124, 16908−16917

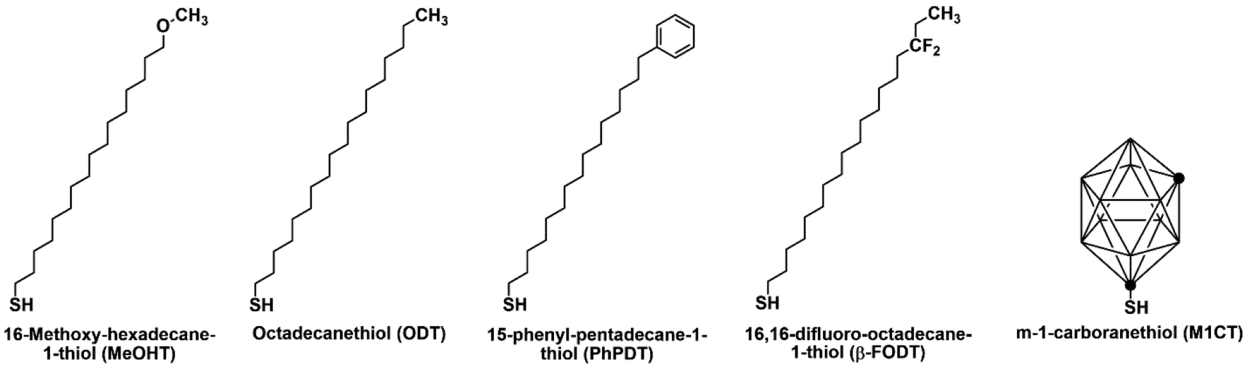

Figure 1. Respective MeOHT, ODT, PhPDT, β-FODT, and M1CT alkanethiol structures.

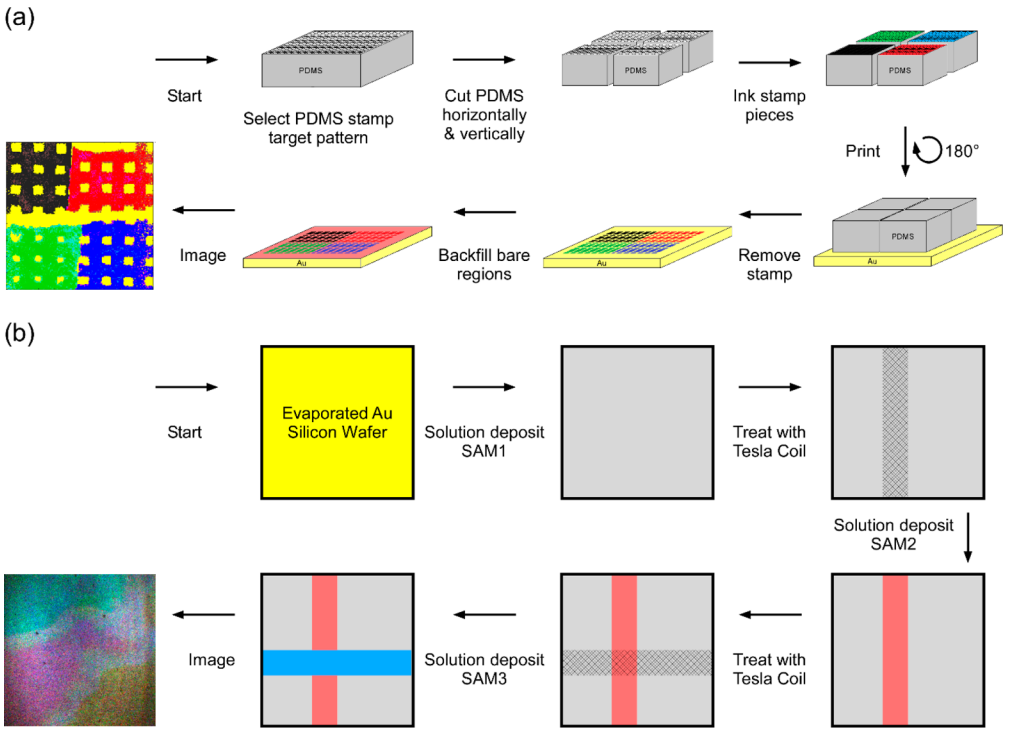

Figure 2. Schematic diagram of the preparation procedure: (a) five-component patterned sample and (b) randomly formed pattern sample.

has been applied in Raman spectroscopy, infrared spectroscopy, nuclear magnetic resonance, mass spectrometry, and so on to determine reaction mechanics, kinetics, and the number and identities of components in a series of related multicomponent mixtures.[39−43,48−55]

Previous results of factor analysis (FA) applied to SFG images demonstrated that it is successful as an alternative method to spectral fitting in generating chemical maps of binary systems.[56] The chemical systems consisted of two different self-assembled monolayers (SAMs) that possessed either very similar or distinctly different vibrational spectra. In addition, FA was successfully applied to data obtained with shorter acquisition times (i.e., weaker signals).

In this study, SFG images of monolayers patterned by microcontact printing using five distinct alkanethiols on gold were acquired by SFG-IM and then analyzed by FA. Utilizing a library consisting of SFG alkanethiol spectra, we determined the chemical components, and their spatial distributions were mapped on the surface. Furthermore, utilizing the alkanethiol library, we used FA to determine the chemical identities and produce chemical maps of a randomly patterned multicomponent alkanethiol SAM. The results demonstrate the capability of FA combined with the spectral library to determine the chemical composition and spatial distribution of organic monolayer species on the surface of multicomponent complex chemical systems analyzed by SFG-IM. Also, FA revealed an unknown surface species, the spectra of which were not contained in the library. Currently, this technique has been applied to a system consisting of five distinct molecules, but it can be extended to larger sample varieties and more complex chemical systems consisting of a larger numbers of species by using a wider spectral range. Isotope labels can also be successfully used due to the ability of FA to resolve spectra at the SFG spectra resolution limit of 5 cm^{-1}.[56]

THEORETICAL BACKGROUND

Sum Frequency Generation (SFG). The theoretical background of SFG and its application has been described previously in detail.[6,28,57] The SFG process here is achieved

https://dx.doi.org/10.1021/acs.jpcc.0c02038
J. Phys. Chem. C 2020, 124, 16908−16917

when two coherent laser beams, a fixed wavelength of 1064 nm (ω_{1064nm}) and a tunable wavelength infrared (ω_{IR}), are spatially and temporally overlapped on a surface to induce a second-order nonlinear polarization. The induced polarization generates the coherent sum frequency beam at the sum of the two input beam frequencies ($\omega_{SF} = \omega_{1064nm} + \omega_{IR}$). When the IR frequency is at a resonance frequency of one of the vibrational modes, a change in the SFG signal is observed.

Factor Analysis. The theoretical background and application of factor analysis (FA) are discussed in detail by Malinowski.[39] A short description of the main steps is presented in the Supporting Information. Factor analysis is a mathematical technique for studying matrices of data. It is a useful method for furnishing the number of components, concentrations, and spectral information via a purely mathematical route.[39] Factor analysis includes principal factor analysis (PFA), which is also known as principal component analysis (PCA), and target factor analysis (TFA). It is performed by taking a data set of interest and obtaining a mathematical solution by decomposition. Each data point of the data set, after decomposition, is expressed as a linear sum of product terms. Because the factor analytical solution is purely mathematical, having no physical or chemical meaning, the resulting matrices are termed "abstract" factors. To acquire chemically recognizable factors, a transformation of the abstract factors is required. Target factor analysis uses target testing as a unique transformation method to test potential factors and to transform the abstract factors into real factors. Target testing serves as a mathematical bridge between abstract and real factors.

EXPERIMENTAL SECTION

Materials and Sample Preparation. The thiol adsorbates used to generate the SAMs were octadecanethiol (ODT), 16-methoxyhexadecane-1-thiol (MeOHT),[58] 16,16-difluoro-octadecane-1-thiol (β-FODT), 15-phenylpentadecane-1-thiol (PhPDT),[59] and carborane-1-thiol (M1CT) as illustrated in Figure 1. All reagents used for SAM formation were either purchased and used as received or synthesized in-house (see the Supporting Information for details, including Figures S1 and S2).

SAMs on gold substrate patterning were achieved by utilizing microcontact printing (μCP). The process of stamp manufacturing for μCP using PDMS has been described previously.[56] The preparation procedure of the five components and the random pattern sample is shown in Figures 2a and 2b, respectively, and is only briefly outlined here. Pure solutions of 20 mM ODT, MeOHT, β-FODT, PhPDT, and M1CT in ethanol were prepared. Pure alkanethiol SAMs samples for target testing library by TFA were prepared by solution deposition for 15 min of the respective alkanethiol solution on evaporated gold silicon wafers. For the preparation of the five-component monolayer sample, a pattern from the PDMS stamp was selected and cut into four pieces. Each piece of the PDMS stamp was inked with a different alkanethiol solution by placing a drop of the respective alkanethiol solution on top of the PDMS stamp and then dried by nitrogen gas. The four PDMS pieces were brought together and carefully placed on the surface of evaporated gold on a silicon wafer. Light pressure was applied to the PDMS stamp and left on the surface for 15 min. After the stamp was removed, the sample was placed into the alkanethiol solution that was not used for stamping to backfill bare gold regions. After 15 min solution deposition, the sample was taken out and rinsed with ethanol and dried with nitrogen.

The random pattern sample was prepared from the same alkanethiol solutions as the five-component and target-test library samples. First, ODT was solution deposited onto a piece of evaporated gold substrate for 15 min, after which it was taken out of solution, rinsed with ethanol, and dried with nitrogen. By use of a hand-held Tesla coil to generate local plasma, a straight line was drawn across the sample while the Tesla coil tip was held at about 1 cm above the sample. After the plasma treatment, the sample was placed into the MeOHT solution for 15 min, after which it was taken out of solution, rinsed with ethanol, and dried with nitrogen. The sample was again treated with plasma in the same manner, but with a straight line drawn perpendicular to the previous plasma treatment. The sample was then placed into the β-FODT solution. After 15 min, it was taken out of solution, rinsed with ethanol, and dried with nitrogen. All samples were rinsed with ethanol solvent and dried with nitrogen gas before taking images.

Sum Frequency Generation Imaging Microscope (SFG-IM). The SFG-IM microscope has been described previously in detail elsewhere.[14,56] Briefly, a picosecond pulsed Nd:YAG laser, with a 20 Hz repetition rate, was used to generate a 1064 nm beam, part of which was used to pump the optical parametric generator/amplifier (OPG/OPA) to produce the tunable mid-IR beam. The incident angles of the 1064 nm and tunable mid-IR beams were set at 60° and 70° from the surface normal, respectively, and generated the SFG beam around 800 nm with an approximate angle of 62.1° from the surface normal. The average energies of the two beams on the surface were about 100 mJ/cm^2 for the 1064 nm beam and 50 mJ/cm^2 for the IR beam. The SFG signal was collected by using an intensified charge-coupled device (ICCD) detector (Roper Scientific) with a 1024 × 1024 pixel chip.

SFG Image Data Processing with Target Factor Analysis. During the SFG imaging, the ICCD detector acquired 71 SFG images sequentially, while the mid-IR frequencies were continuously scanned from 2747 to 3102 cm^{-1} at 1000 laser shots per image. Each SFG image is an integration of a 5 cm^{-1} interval. No processing of the presented SFG images was performed except for background correction. Once the set of images was acquired by using ImageJ software, the images were staked according to decreasing IR wavenumber. The image stack was divided into a square region of interests (ROIs) of 5 by 5 pixels, which corresponds to 6.5 by 6.5 μm, and the vibrational spectra were extracted from each ROI. By use of MATLAB, the extracted spectra were normalized and compiled into a data matrix in a specified sequence, where each ROI spectrum is a column of the data matrix, on which FA was performed. The SFG image stacks of pure solution deposited alkanethiol samples were not divided into ROIs, but the SFG spectra from the whole image were exacted and compiled into a library matrix in MATLAB, containing pure component spectra for TFA.

To determine the number of significant abstract factors necessary to reconstruct the data, the data matrix was decomposed via PFA and analyzed by the factor (empirical) indicator function (IND) (see the Supporting Information for details on IND). To produce transformed real factors and their corresponding chemical maps, the data matrix was then analyzed by TFA. The test (target) spectra from the spectra

https://dx.doi.org/10.1021/acs.jpcc.0c02038
J. Phys. Chem. C 2020, 124, 16908−16917

matrix library were used to produce the transformation matrix by converting significant abstract factors into physically significant factors. To confirm that the test spectra is a real factor in the chemical system, a SPOIL function was used to evaluate all the target spectra in the library used (see the Supporting Information for details on SPOIL).[39] The row matrix obtained from the target transformation contained the transformed (predicted) real factors, and the column matrix contained the component weights of the corresponding transformed real factors. The component weights of each real factor were used to produce the reconstructed chemical maps. The chemical maps were normalized and constrained to positive values only, with no other constraints or processing. The MATLAB codes used were modified PFA and TFA codes provided by Malinowski.[39]

RESULTS AND DISCUSSION

The SFG spectra of pure solution deposited alkanethiols monolayers on a gold substrate that formed the SFG spectra

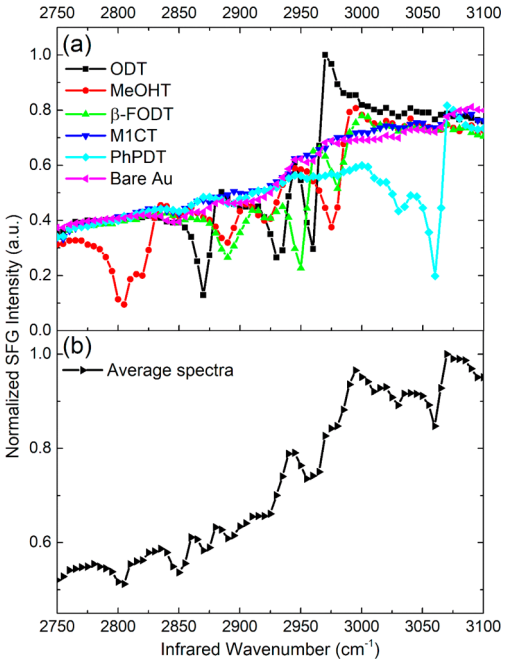

Figure 3. (a) SFG spectra of octadecanethiol (ODT), 16-methoxy-hexadecane-1-thiol (MeOHT), 16,16-difluorooctadecane-1-thiol (*β*-FODT), 15-phenylpentadecane-1-thiol (PhPDT), m-1-carboranethiol (M1CT), and bare Au compared to (b) averaged SFG signal.

"thiol library" were ODT, MeOHT, *β*-FODT, PhPDT, M1CT, and bare gold, shown in Figure 3a. These alkanethiol spectra exhibit some distinct vibrational resonances in the C−H stretching region, 2750−3100 cm^{-1}, that can be used to distinguish the alkanethiols, except for M1CT which has no distinct vibrational bands in the 2750−3100 cm^{-1} region. MeOHT contains a distinct vibrational symmetric stretch of the terminal methoxy ($-OCH_3$) group as a doublet at 2805/2825 cm^{-1}, ODT has a CH_3 symmetric at 2870 cm^{-1}, and PhPDT has aromatic ring stretching resonances between 3030 and 3060 cm^{-1} that do not overlap with any other presented vibrational bands. The resonant vibrational stretches of the alkanethiols in the 2880−3000 cm^{-1} range contain a significant amount of peak overlap. In the SFG images contrast is observed when there is an observable SFG signal intensity

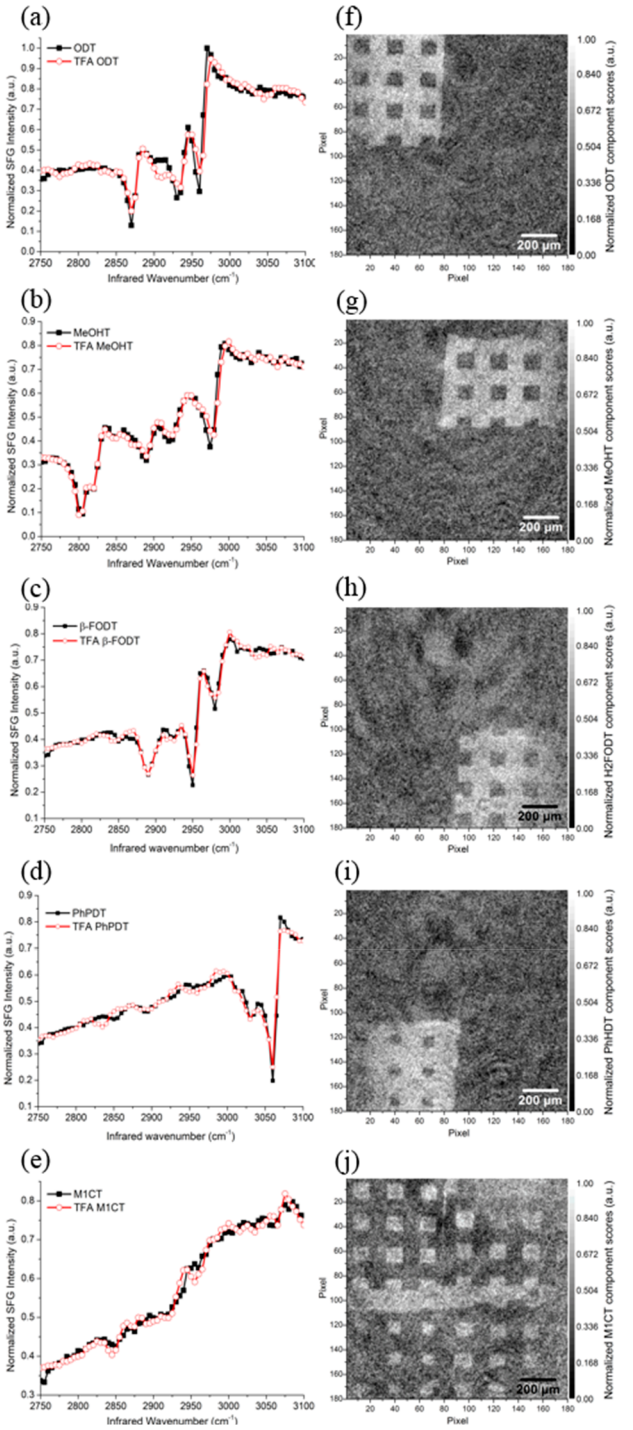

Figure 4. SFG spectra overlaid with the corresponding target transformed spectra predicted by TFA: (a) ODT, (b) MeOHT, (c) *β*-FODT, (d) PhPDT, and (e) M1CT. Corresponding reconstructed TFA chemical images of (f) ODT, (g) MeOHT, (h) *β*-FODT, (i) PhPDT, and (j) M1CT. The lighter region indicates the target SAMs. The scale bar is 200 *μ*m.

difference between the different monolayers. At frequencies where little or no relative signal difference exists, poor image contrast is observed. In the average SFG signal of the five alkanethiols, shown in Figure 3b, the majority of the resonant peaks overlap and cannot be identified. To spectrally fit the average alkanethiol spectra to the general SFG equation, the spectral fitting would require at least 14 terms in the equation,

https://dx.doi.org/10.1021/acs.jpcc.0c02038
J. Phys. Chem. C 2020, 124, 16908−16917

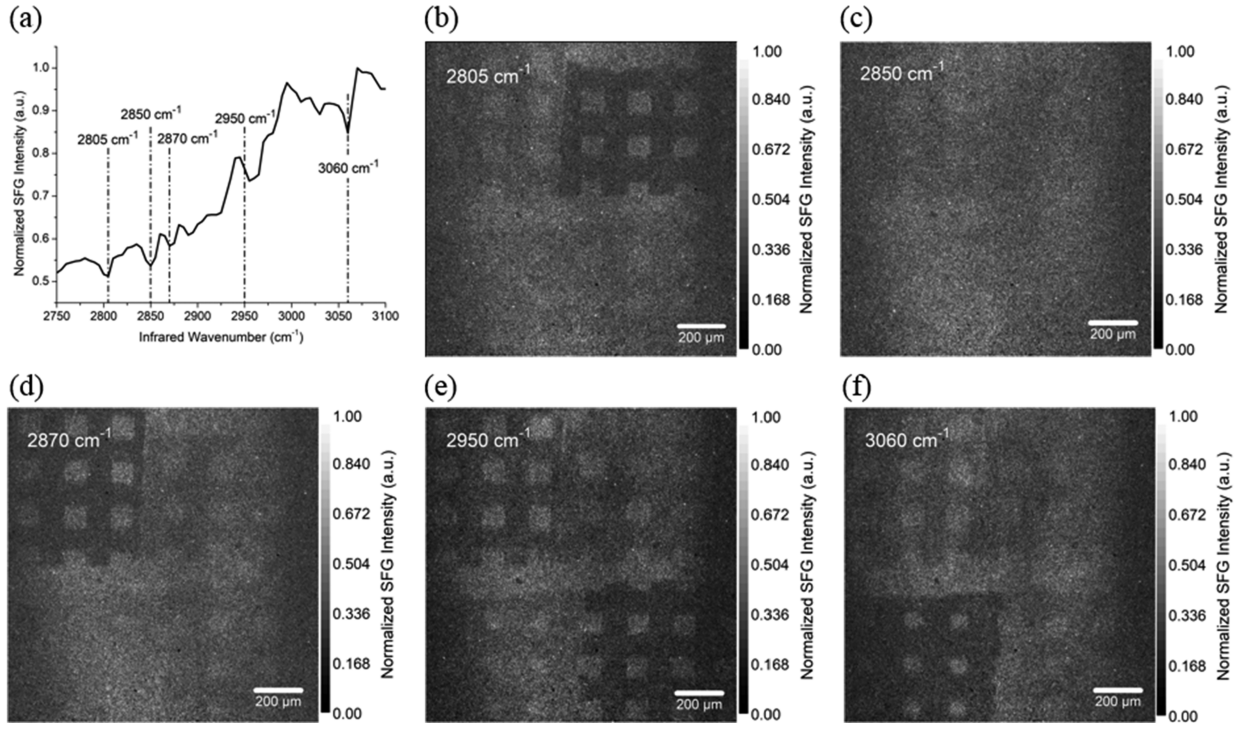

Figure 5. Normalized SFG spectrum (a), averaged over the full image, and images of the five-component sample at (b) 2805, (c) 2850, (d) 2870, (e) 2950, and (f) 3060 cm^{-1}. The scale bar is 200 μm.

which makes it practically impossible to obtain a good fit. Even if the monolayers are spatially separated, the areas where the different alkanethiols meet or overlap, spectral fitting is complicated. For a more realistic sample with unknown spatial distribution, the fitting must be more robust. Furthermore, spectra from smaller ROI have much lower S/N (see Figure S3), exasperating the spectral fitting approach.

Five-Component Patterned Sample. Analyzing the SFG image data matrix of the five-component patterned sample with PFA resulted in 71 abstract factors, due to 71 frequency data points per spectrum. The IND function indicated seven significant abstract factors that account for 97.7% of the data variance. The rest of the abstract factors that account for 2.3% were verified to contain only noise and discarded. Target testing of the thiol library to the seven significant abstract factors confirmed that all five of the tested alkanethiols were real factors of the analyzed data with their corresponding SPOIL values less than 20. This confirmed that an independently prepared library is valid to test unknown samples. Target-transformed real factors by TFA, shown in Figure 4a–e, overlapped well with the corresponding SFG spectra, indicating that TFA can successfully reconstruct decomposed SFG spectra. The images in Figure 4f–j are the TFA resulting in chemical maps showing the spatial distribution of the real factors. The chemical maps were constructed by mapping back the component weights (see Supporting Information eq S7) of each target transformed real factor in each of the 6.5-by-6.5 μm ROIs. The lighter shaded region of each image in Figure 4f–j corresponds to the ODT, MeOHT, β-FODT, PhPDT, and M1CT region, respectively. Upon comparison of the TFA chemical maps to the selected single-wavelength SFG images (Figure 5b–f), the observed image contrast in the SFG images is not specific to just one SAM but contains some contrast of all SAMs.

The normalized SFG spectrum averaged from the five-component image stack is shown in Figure 5a. From the averaged SFG spectrum it is difficult to determine the number of different SAMs on the surface or their identities. To visualize the distribution of the alkanethiols, selected single-wavelength SFG images of the five-component sample are shown in Figure 5b–f. The observed contrast in the SFG images (Figure 5c–f) is due to the vibrational contrast in the SFG spectra, where the darker region of the images correlate to the resonant peaks of the SAMs on the surface at the specified frequency. A lack of unique image contrast is observed when the imaged alkanethiols show little to no vibrational resonance or very similar vibrational intensity at the specified frequency; such an example is shown in Figure 5b. The image contrast observed in the presented single-wavelength SFG images (Figure 5b–f) is nonspecific or absent. The different contrast intensities can be attributed to different monolayer coverage of the same SAM or weaker (residual) signal from other SAMs. It is not enough to rely just on single-wavelength images to determine the spatial distribution of the monolayer due to the nonspecific contrast. By utilizing the entire spectral range, rather than a single wavelength, we determined the true identity and spatial distribution of the SAMs.

It was determined that the observed darker region in the upper right quarter of the SFG image taken at 2805 cm^{-1} (Figure 5c) corresponds to the MeOHT covered surface, which has a symmetric methoxy stretch at that frequency. The darker region in the upper left quarter of the 2870 cm^{-1} SFG image (Figure 5d) corresponds to the ODT region of the surface, which has a methyl symmetric stretch at that frequency. The β-FODT SAM region is the darker area in the bottom right quarter of the 2950 cm^{-1} image (Figure 5e). The observed image contrast in the rest of the image is due to the nonresonant SFG signal difference between the stamped ODT and MeOHT regions and the backfilled M1CT region,

https://dx.doi.org/10.1021/acs.jpcc.0c02038
J. Phys. Chem. C 2020, 124, 16908–16917

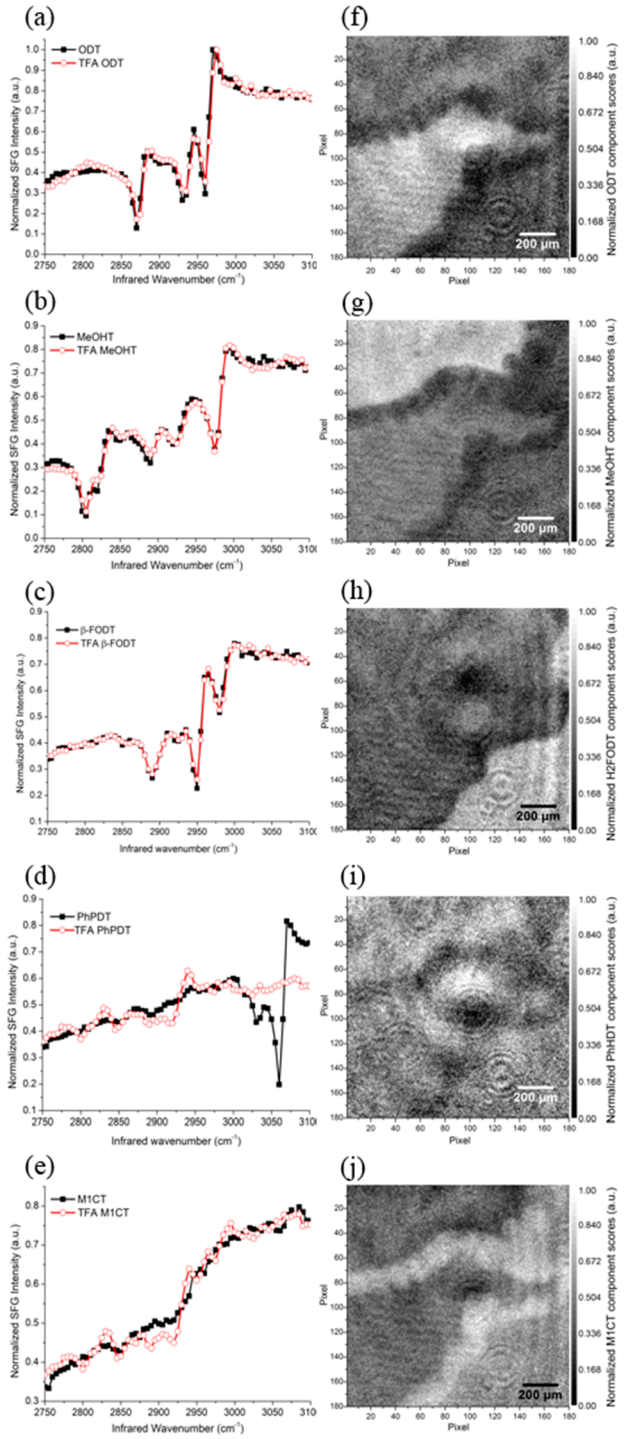

Figure 6. SFG spectra overlaid with the corresponding target transformed spectra predicted by TFA: (a) ODT, (b) MeOHT, (c) β-FODT, (d) PhPDT, and (e) M1CT. The corresponding reconstructed TFA chemical images of (f) ODT, (g) MeOHT, (h) β-FODT, (i) PhPDT, and (j) M1CT. The lighter region indicates the target SAMs. The scale bar is 200 μm.

where M1CT has a higher nonresonant signal than ODT and MeOHT. The darker region in the bottom left quarter of the 3060 cm^{-1} images (Figure 5f) represents the PhPDT monolayer region. Because M1CT does not contain any strong resonant vibrational bends in the selected frequency range, but mainly a nonresonant signal, it is observed as the lightest region in Figure 5e. The spatial positions of the alkanethiols were verified by selecting the corresponding regions and analyzing the extracted vibrational spectra.

The TFA chemical maps represent the distribution of the respective monolayers as the lighter shaded region of the image, which corresponds to the darker shaded regions of the SFG images. The chemical map of ODT (Figure 4f), the lighter color corresponding to the ODT distribution, shows that ODT is present in the upper right corner of the image and corresponds to the darker shaded upper left region of the image in Figure 5d. Similarly, the TFA chemical maps of MeOHT, β-FODT, PhPDT, and M1CT in Figure 4g–j, respectively, are in very good agreement with the SFG images shown in Figure 5b–f, indicating the capability of FA to deconvolute the spectra via SVD, predict the chemical composition, and generate chemical maps via target testing. Spectral decomposition with target testing allows the possibility to use SFG imaging to analyze more complex samples, containing multiple chemical species.

Random Pattern Three-Component Sample. To assess the performs of TFA on a more natural system, where the spatial distribution of the molecules is unknown, samples of randomly formed ODT, MeOHT, and β-FODT SAMs were prepared. The SFG image stack was acquired and processed in the same manner as the patterned five-component data. Principal factor analysis indicated that six significant abstract factors account for 98.4% of data variance. Target testing of the alkanethiol library indicated that ODT, MeOHT, and β-FODT were real factors of the data analyzed, with corresponding SPOIL values below 20, while M1CT, PhPDT, and bare Au had SPOIL values above 30, indicating that they were not real factors in the analyzed data. Target transformed real factors by TFA are shown in Figure 6a–e, overlapped with the corresponding SFG spectra. TFA predicted spectra were in good agreement with the corresponding SFG spectra of ODT, MeOHT, and β-FODT as shown in Figure 6a–c, respectively. The corresponding TFA chemical maps of ODT, MeOHT, and β-FODT are shown in Figure 6f–h, respectively, where the lighter region of each map represents the respective SAMs coverage. TFA correctly identified that PhPDT was not a real factor since PhPDT was not used in the preparation of the sample. Aromatic ring stretching between 3030 and 3060 cm^{-1} was not present in any of the abstract factors, and no combination of significant factors will reproduce spectra resembling PhPDT. Figure 6d shows PhPDT SFG spectra overlapped with the attempted TFA target transformation using PhPDT as a target, with the corresponding chemical map (Figure 6i) showing a very weak image contrast as expected. Similarly, the SFG spectrum of M1CT did not overlap well with the TFA predicted spectrum shown in Figure 6e. These results indicate that TFA has the sensitivity to distinguish spectral band changes and correctly (positively) determine true chemical components.

The averaged SFG spectrum and selected SFG images representing the main vibrational frequency of ODT, MeOHT, and β-FODT of the random sample are presented in Figure 7. The image in Figure 7b–d was taken at the IR frequencies of 2805, 2870, and 2950 cm^{-1}, where the darker regions of each image represent the MeOHT, ODT, and β-FODT region, respectively. The SAMs pattern observed in the presented SFG images was unexpected. Utilizing a hand-held Tesla coil creates a unique, nonreproducible pattern since there is little control over the intensity and distribution of the local plasma generated. Comparison of the TFA generated ODT,

https://dx.doi.org/10.1021/acs.jpcc.0c02038
J. Phys. Chem. C 2020, 124, 16908–16917

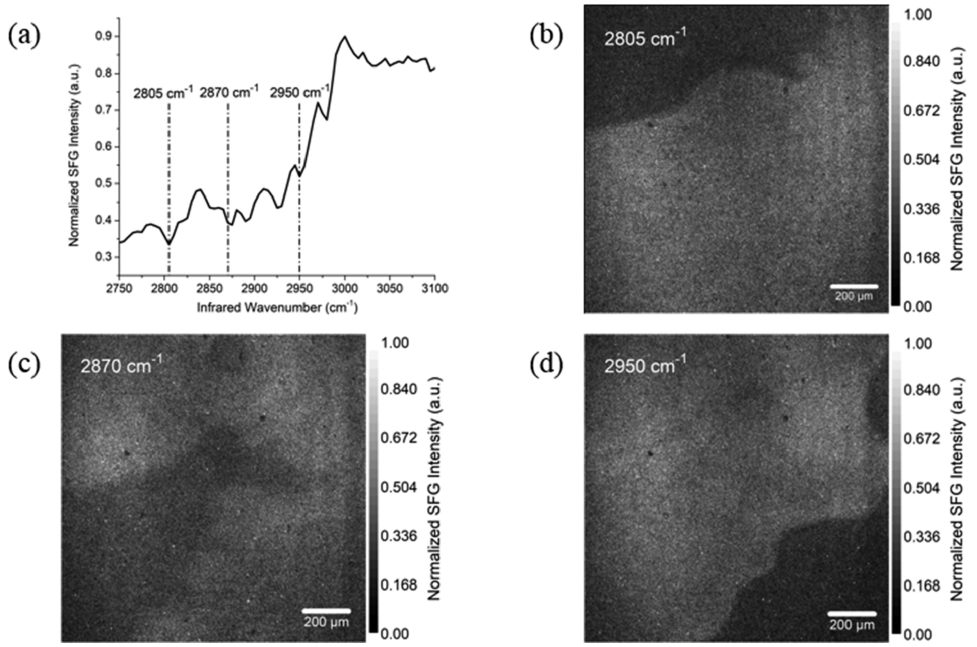

Figure 7. Normalized SFG spectrum (a) averaged over the full image. Images of the random pattern sample at (b) 2805, (c) 2870, and (d) 2950 cm^{-1}.

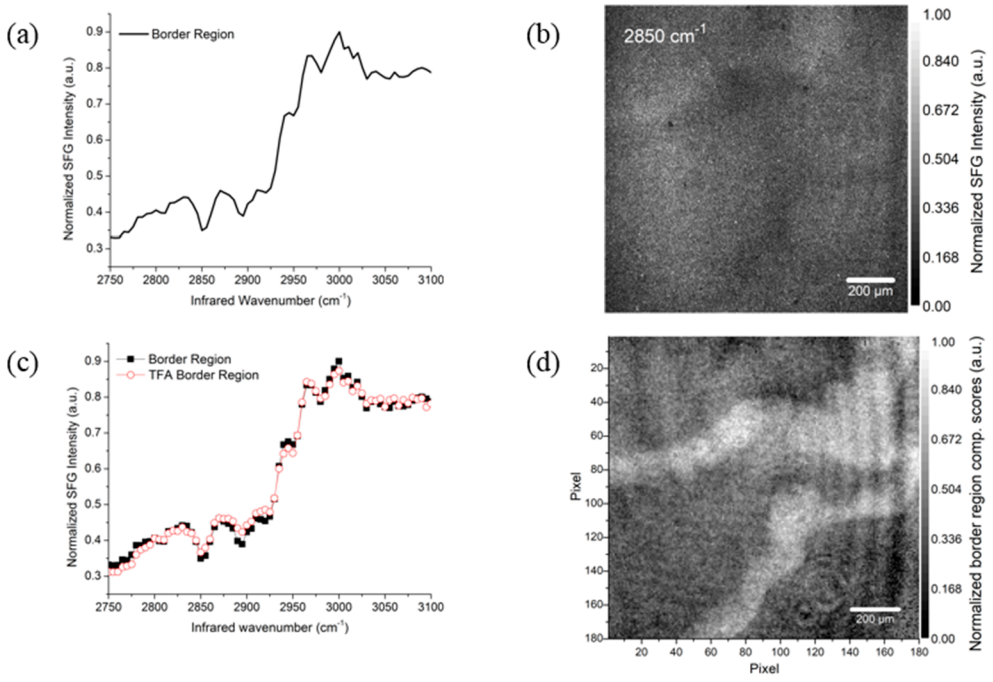

Figure 8. (a) SFG spectrum extracted from the border region of the random pattern sample. (b) SFG image at 2850 cm^{-1}. (c) Border region SFG spectra overlaid with the corresponding target transformed spectra predicted by TFA. (d) The corresponding chemical map.

MeOHT, and β-FODT chemical maps (Figure 6f–h) with the SFG images in Figure 7b–d showed good agreement. The possibility of correctly identifying the real factors and producing chemical images that correspond to the respective SFG image chemical contrast make TFA an important tool for SFG image analysis.

In the ODT, MeOHT, and β-FODT TFA images (Figure 6f–h) there is an observable chemical contrast between the ODT, MeOHT, and β-FODT regions as the darkest region of the images. Surprisingly, the contrast is also apparent in Figure 6i as the darker region and Figure 6j as the lightest region. This observed border region contained spectral features that were not identified as one of the five alkanethiols used for target testing. An SFG spectrum extracted from the border region is shown in Figure 7a. A faint peak at 2810 cm^{-1} and a relatively large peak at 2850 cm^{-1} are observed in the MeOHT spectrum as the methoxy symmetric and CH_2 symmetric stretches, respectively. The spectrum also contains peaks at 2895, 2950, and 2980 cm^{-1} which are observed in β-FODT spectrum as the CH_2 symmetry, CH_3 symmetric, and CH_3 asymmetric stretches, respectively.[60−64] The ODT CH_3 resonant peaks at 2870 and 2960 cm^{-1} are not observed in the border region,

https://dx.doi.org/10.1021/acs.jpcc.0c02038
J. Phys. Chem. C 2020, 124, 16908−16917

which could be the result that the ODT molecules were altogether removed from the surface during the sample preparation or were modified to some extent that effects the CH_3 functional group. The spectrum shows a strong CH_2 symmetric stretch at 2850 cm^{-1}, which is present as a minor dip in most of the alkanethiol spectra (Figure 3a) and indicates the possibility of gauche defects in the SAMs.[65,66] Thus, the border region possibly contains highly disorder MeOHT and β-FODT molecules. Because the application of TFA in this study was purely qualitative, the quantification of MeOHT and β-FODT in the border region was not attempted. Utilizing a calibration curve with correct targets, we can use TFA for quantifying of monolayer mixing (see the Supporting Information TFA Quantification of Monolayer Mixing). The border region is faintly visible as the darker region in the SFG image at 2850 cm^{-1}, shown in Figure 7b. The slightly larger CH_2 symmetric stretch in the border region compared to the other regions is responsible for the observed contrast in Figure 7b. This behavior of the SAMs is believed to be the result of the random pattern generation method used to prepare the sample. The observed changes need to be studied to determine the changes that the alkanethiols undergo during the sample preparation procedure. Target testing the extracted SFG spectrum from the border region returned a SPOIL value below 20, indicating that it was a real factor. The target transformed spectra and the corresponding chemical map are shown in Figures 8c and 8d, respectively, where the lighter region of Figure 8d corresponds to the border region.

CONCLUSIONS

The presented work has demonstrated that FA can be successfully utilized with a spectral library to determine monolayer identities and their spatial distribution. In this study, the chemical systems analyzed were patterned five components and a random pattern. By use of a spectral library as a target test for TFA, the correct identification and spatial distribution of the monolayers were made possible. Also, FA was able to identify an unknown monolayer region, the vibrational spectra of which were not present in the target library.

Although the above observations demonstrate the potential of this technique for chemical identification and chemical map generation, it can be further extended in several ways. First, the target test library can be expanded to include more variety of vibrational spectra by using isotopic labels (^{13}C, ^{2}H, ^{18}O, etc.). This can potentially double or triple the number of molecules studied. Second, the infrared wavelength resolution can be increased to obtain narrower vibrational bands, which will allow the resolution of overlapping bands. Third, imaging resolution can be improved to resolve finer features. Fourth, a wider range of wavelengths can also be used. In addition, the present analysis forms the basis for the analysis of complex components in the SFG spectra, including phase and amplitude of the various components.

ASSOCIATED CONTENT

Supporting Information

The Supporting Information is available free of charge at https://pubs.acs.org/doi/10.1021/acs.jpcc.0c02038.

Materials and adsorbate sources, synthesis of 16,16-difluorooctadecane-1-thiol (β-FODT), ^{1}H and ^{13}C NMR spectra of 16,16-difluorooctadecane-1-thiol (β-FODT), factor analysis details, SPOIL function description, SFG spectra extracted from different ROI sizes, and TFA quantification of monolayer mixing (PDF)

AUTHOR INFORMATION

Corresponding Author

Steven Baldelli − *Department of Chemistry, University of Houston, Houston, Texas 77204-5003, United States;* orcid.org/0000-0002-5747-259X; Email: sbaldelli@uh.edu

Authors

Aleksandr A. Pikalov − *Department of Chemistry, University of Houston, Houston, Texas 77204-5003, United States*

Tianlang Yu − *Department of Chemistry, University of Houston, Houston, Texas 77204-5003, United States;* orcid.org/0000-0001-6218-5694

Daniela Rodriguez − *Department of Chemistry, University of Houston, Houston, Texas 77204-5003, United States*

Han Ju Lee − *Department of Chemistry, University of Houston, Houston, Texas 77204-5003, United States*

T. Randall Lee − *Department of Chemistry, University of Houston, Houston, Texas 77204-5003, United States;* orcid.org/0000-0001-9584-8861

Complete contact information is available at: https://pubs.acs.org/10.1021/acs.jpcc.0c02038

Notes

The authors declare no competing financial interest.

ACKNOWLEDGMENTS

The authors thank Prof. C. D. Bain for suggesting to utilize principal component analysis for SFG image analysis. We also thank Syed Alamadar Hussain Shah for assistance and in-depth discussions. S.B. gratefully acknowledges NSF (1610453) for providing the funds for this project. T.R.L. thanks the National Science Foundation (CHE-1710561), the Robert A. Welch Foundation (E-1320), and the Texas Center for Superconductivity for support.

REFERENCES

(1) Florsheimer, M.; Brillert, C.; Fuchs, H. Chemical imaging of interfaces by sum-frequency generation. *Mater. Sci. Eng., C* **1999**, *8*−*9*, 335−341.

(2) Hoffmann, D. M. P.; Kuhnke, K.; Kern, K. Chemical imaging of structured SAMs with a novel SFG microscope. *Proc. SPIE* **2002**, *4812*, 82−90.

(3) Cimatu, K.; Baldelli, S. Sum frequency generation microscopy of microcontact-printed mixed self-assembled monolayers. *J. Phys. Chem. B* **2006**, *110* (4), 1807−1813.

(4) Shen, Y. R. Surface-Properties Probed by Second-Harmonic and Sum-Frequency Generation. *Nature* **1989**, *337* (6207), 519−525.

(5) Zhu, X. D.; Suhr, H.; Shen, Y. R. Surface Vibrational Spectroscopy by Infrared-Visible Sum Frequency Generation. *Phys. Rev. B: Condens. Matter Mater. Phys.* **1987**, *35* (6), 3047−3050.

(6) Bain, C. D. Sum-Frequency Vibrational Spectroscopy of the Solid-Liquid Interface. *J. Chem. Soc., Faraday Trans.* **1995**, *91* (9), 1281−1296.

(7) Fang, M.; Baldelli, S. Surface-Induced Heterogeneity Analysis of an Alkanethiol Monolayer on Microcrystalline Copper Surface Using Sum Frequency Generation Imaging Microscopy. *J. Phys. Chem. C* **2017**, *121* (3), 1591−1601.

(8) Kuhnke, K.; Hoffmann, D. M. P.; Wu, X. C.; Bittner, A. M.; Kern, K. Chemical imaging of interfaces by sum-frequency generation microscopy: Application to patterned self-assembled monolayers. *Appl. Phys. Lett.* **2003**, *83* (18), 3830−3832.
(9) Hoffmann, D. M. P.; Kuhnke, K.; Kern, K. Sum-frequency generation microscope for opaque and reflecting samples. *Rev. Sci. Instrum.* **2002**, *73* (9), 3221−3226.
(10) Shen, Y. R. Surfaces Probed by Nonlinear Optics. *Surf. Sci.* **1994**, *299* (1−3), 551−562.
(11) Su, X. C.; Cremer, P. S.; Shen, Y. R.; Somorjai, G. A. High-pressure CO oxidation on Pt(111) monitored with infrared-visible sum frequency generation (SFG). *J. Am. Chem. Soc.* **1997**, *119* (17), 3994−4000.
(12) Cremer, P. S.; Su, X. C.; Shen, Y. R.; Somorjai, G. A. Ethylene hydrogenation on Pt(111) monitored in situ at high pressures using sum frequency generation. *J. Am. Chem. Soc.* **1996**, *118* (12), 2942−2949.
(13) Chen, Z.; Gracias, D. H.; Somorjai, G. A. Sum frequency generation (SFG)-surface vibrational spectroscopy studies of buried interfaces: catalytic reaction intermediates on transition metal crystal surfaces at high reactant pressures; polymer surface structures at the solid-gas and solid-liquid interfaces. *Appl. Phys. B: Lasers Opt.* **1999**, *68* (3), 549−557.
(14) Cimatu, K. A.; Baldelli, S. Chemical Microscopy of Surfaces by Sum Frequency Generation Imaging. *J. Phys. Chem. C* **2009**, *113* (38), 16575−16588.
(15) Fang, M.; Baldelli, S. Grain Structures and Boundaries on Microcrystalline Copper Covered with an Octadecanethiol Monolayer Revealed by Sum Frequency Generation Microscopy. *J. Phys. Chem. Lett.* **2015**, *6* (8), 1454−1460.
(16) Raghunathan, V.; Han, Y.; Korth, O.; Ge, N. H.; Potma, E. O. Rapid vibrational imaging with sum frequency generation microscopy. *Opt. Lett.* **2011**, *36* (19), 3891−3893.
(17) Smith, K. A.; Conboy, J. C. A Simplified Sum-Frequency Vibrational Imaging Setup Used for Imaging Lipid Bilayer Arrays. *Anal. Chem.* **2012**, *84* (19), 8122−8126.
(18) Sahlin, J. J.; Peppas, N. A. Near-field FTIR imaging: A technique for enhancing spatial resolution in FTIR microscopy. *J. Appl. Polym. Sci.* **1997**, *63* (1), 103−110.
(19) Kazarian, S. G.; Chan, K. L. A. Applications of ATR-FTIR spectroscopic imaging to biomedical samples. *Biochim. Biophys. Acta, Biomembr.* **2006**, *1758* (7), 858−867.
(20) Ray, K.; McCreery, R. L. Spatially resolved Raman spectroscopy of carbon electrode surfaces: Observations of structural and chemical heterogeneity. *Anal. Chem.* **1997**, *69* (22), 4680−4687.
(21) Treado, P. J.; Govil, A.; Morris, M. D.; Sternitzke, K. D.; Mccreery, R. L. Hadamard-Transform Raman Microscopy of Laser-Modified Graphite-Electrodes. *Appl. Spectrosc.* **1990**, *44* (8), 1270−1275.
(22) Zumbusch, A.; Holtom, G. R.; Xie, X. S. Three-dimensional vibrational imaging by coherent anti-Stokes Raman scattering. *Phys. Rev. Lett.* **1999**, *82* (20), 4142−4145.
(23) Cheng, J. X.; Volkmer, A.; Book, L. D.; Xie, X. S. An epi-detected coherent anti-stokes raman scattering (E-CARS) microscope with high spectral resolution and high sensitivity. *J. Phys. Chem. B* **2001**, *105* (7), 1277−1280.
(24) Cheng, J. X.; Volkmer, A.; Book, L. D.; Xie, X. S. Multiplex coherent anti-stokes Raman scattering microspectroscopy and study of lipid vesicles. *J. Phys. Chem. B* **2002**, *106* (34), 8493−8498.
(25) Cheng, J. X.; Xie, X. S. Coherent anti-Stokes Raman scattering microscopy: Instrumentation, theory, and applications. *J. Phys. Chem. B* **2004**, *108* (3), 827−840.
(26) Potma, E. O.; Xie, X. S.; Muntean, L.; Preusser, J.; Jones, D.; Ye, J.; Leone, S. R.; Hinsberg, W. D.; Schade, W. Chemical imaging of photoresists with coherent anti-Stokes Raman scattering (CARS) microscopy. *J. Phys. Chem. B* **2004**, *108* (4), 1296−1301.
(27) Shen, Y. R. Basic Theory of Surface Sum-Frequency Generation. *J. Phys. Chem. C* **2012**, *116* (29), 15505−15509.
(28) Wang, H. F.; Gan, W.; Lu, R.; Rao, Y.; Wu, B. H. Quantitative spectral and orientational analysis in surface sum frequency generation vibrational spectroscopy (SFG-VS). *Int. Rev. Phys. Chem.* **2005**, *24* (2), 191−256.
(29) Jang, J. H.; Jacob, J.; Santos, G.; Lee, T. R.; Baldelli, S. Image Contrast in Sum Frequency Generation Microscopy Based on Monolayer Order and Coverage. *J. Phys. Chem. C* **2013**, *117* (29), 15192−15202.
(30) Cimatu, K.; Moore, H. J.; Barriet, D.; Chinwangso, P.; Lee, T. R.; Baldelli, S. Sum frequency generation imaging microscopy of patterned self-assembled monolayers with terminal -CH3, -OCH3, -CF2CF3, -C═C, -phenyl, and -cyclopropyl groups. *J. Phys. Chem. C* **2008**, *112* (37), 14529−14537.
(31) Santos, G.; Baldelli, S. Scale Dependence of the Orientation and Conformation Distribution Analysis of a Molecular Mono layer Using Sum Frequency Generation Imaging Microscopy. *J. Phys. Chem. C* **2012**, *116* (49), 25874−25887.
(32) Cimatu, K.; Moore, H. J.; Lee, T. R.; Baldelli, S. Sum frequency generation imaging of microcontact-printed monolayers derived from aliphatic dithiocarboxylic acids: Contrast based on terminal-group orientation. *J. Phys. Chem. C* **2007**, *111* (32), 11751−11755.
(33) Rey, N. G.; Weissenborn, E.; Schulze-Zachau, F.; Gochev, G.; Braunschweig, B. Quantifying Double-Layer Potentials at Liquid Gas Interfaces from Vibrational Sum-Frequency Generation. *J. Phys. Chem. C* **2019**, *123* (2), 1279−1286.
(34) Novakovic, D.; Saarinen, J.; Rojalin, T.; Antikainen, O.; Fraser-Miller, S. J.; Laaksonen, T.; Peltonen, L.; Isomaki, A.; Strachan, C. J. Multimodal Nonlinear Optical Imaging for Sensitive Detection of Multiple Pharmaceutical Solid-State Forms and Surface Transformations. *Anal. Chem.* **2017**, *89* (21), 11460−11467.
(35) Zheng, D. S.; Lu, L. Y.; Kelly, K. F.; Baldelli, S. Chemical Imaging of Self-Assembled Monolayers on Copper Using Compressive Hyperspectral Sum Frequency Generation Microscopy. *J. Phys. Chem. B* **2018**, *122* (2), 464−471.
(36) Huang, S. X.; Makarem, M.; Kiemle, S. N.; Hamedi, H.; Sau, M.; Cosgrove, D. J.; Kim, S. H. Inhomogeneity of Cellulose Microfibril Assembly in Plant Cell Walls Revealed with Sum Frequency Generation Microscopy. *J. Phys. Chem. B* **2018**, *122* (19), 5006−5019.
(37) Lee, C. M.; Kafle, K.; Huang, S. X.; Kim, S. H. Multimodal Broadband Vibrational Sum Frequency Generation (MM-BB-V-SFG) Spectrometer and Microscope. *J. Phys. Chem. B* **2016**, *120* (1), 102−116.
(38) Nickolov, Z. S.; Britt, D. W.; Miller, J. D. Sum-frequency spectroscopy analysis of two-component Langmuir monolayers and the associated interfacial water structure. *J. Phys. Chem. B* **2006**, *110* (31), 15506−15513.
(39) Malinowski, E. R. *Factor Analysis in Chemistry*, 3rd ed.; Wiley: New York, 2002; p xviii, 414 pp.
(40) Mccue, M.; Malinowski, E. R. Target Factor Analysis of Infrared-Spectra of Multicomponent Mixtures. *Anal. Chim. Acta* **1981**, *133* (2), 125−136.
(41) Ngo, D.; Baldelli, S. Adsorption of Dimethyldodecylamine Oxide and Its Mixtures with Triton X-100 at the Hydrophilic Silica/Water Interface Studied Using Total Internal Reflection Raman Spectroscopy. *J. Phys. Chem. B* **2016**, *120* (48), 12346−12357.
(42) Woods, D. A.; Petkov, J.; Bain, C. D. Surfactant adsorption by total internal reflection Raman spectroscopy. Part III: Adsorption onto cellulose. *Colloids Surf., A* **2011**, *391* (1−3), 10−18.
(43) Day, J. P. R.; Campbell, R. A.; Russell, O. P.; Bain, C. D. Adsorption kinetics in binary surfactant mixtures studied with external reflection FTIR spectroscopy. *J. Phys. Chem. C* **2007**, *111* (25), 8757−8774.
(44) Lewis, I. R.; Edwards, H. G. M. *Handbook of Raman Spectroscopy: From the Research Laboratory to the Process Line*; Marcel Dekker: New York, 2001; p xiii, 1054 pp.
(45) Geladi, P.; Sethson, B.; Nystrom, J.; Lillhonga, T.; Lestander, T.; Burger, J. Chemometrics in spectroscopy - Part 2. Examples. *Spectrochim. Acta, Part B* **2004**, *59* (9), 1347−1357.

https://dx.doi.org/10.1021/acs.jpcc.0c02038
J. Phys. Chem. C 2020, 124, 16908−16917

(46) Larrechi, M. S.; Callao, M. P. Strategy for introducing NIR spectroscopy and multivariate calibration techniques in industry. *TrAC, Trends Anal. Chem.* **2003**, *22* (9), 634−640.
(47) vandenBroek, W. H. A. M.; Derks, E. P. P. A.; vandeVen, E. W.; Wienke, D.; Geladi, P.; Buydens, L. M. C. Plastic identification by remote sensing spectroscopic NIR imaging using kernel partial least squares (KPLS). *Chemom. Intell. Lab. Syst.* **1996**, *35* (2), 187−197.
(48) Koons, J. M.; Ellis, P. D. Applicability of Factor-Analysis in Solid-State Nmr. *Anal. Chem.* **1995**, *67* (23), 4309−4315.
(49) Weiner, P. H.; Howery, D. G. Factor-Analysis of Some Chemical and Physical Influences in Gas-Liquid Chromatography. *Anal. Chem.* **1972**, *44* (7), 1189−1194.
(50) Mccue, M.; Malinowski, E. R. Target Factor-Analysis of the Ultraviolet-Spectra of Unresolved Liquid-Chromatographic Fractions. *Appl. Spectrosc.* **1983**, *37* (5), 463−469.
(51) Malinowski, E. R.; Mccue, M. Qualitative and Quantitative-Determination of Suspected Components in Mixtures by Target Transformation Factor-Analysis of Their Mass-Spectra. *Anal. Chem.* **1977**, *49* (2), 284−287.
(52) Shao, L. M.; Griffiths, P. R. Information Extraction from a Complex Multicomponent System by Target Factor Analysis. *Anal. Chem.* **2010**, *82* (1), 106−114.
(53) Carvalho, A. R.; Wattoom, J.; Zhu, L. F.; Brereton, R. G. Combined kinetics and iterative target transformation factor analysis for spectroscopic monitoring of reactions. *Analyst* **2006**, *131* (1), 90−97.
(54) Zhu, L. F.; Brereton, R. G.; Thompson, D. R.; Hopkins, P. L.; Escott, R. E. A. On-line HPLC combined with multivariate statistical process control for the monitoring of reactions. *Anal. Chim. Acta* **2007**, *584* (2), 370−378.
(55) Pachuta, S. J. Enhancing and automating TOF-SIMS data interpretation using principal component analysis. *Appl. Surf. Sci.* **2004**, *231*, 217−223.
(56) Pikalov, A. A.; Ngo, D.; Lee, H. J.; Lee, T. R.; Baldelli, S. Sum Frequency Generation Imaging Microscopy of Self-Assembled Monolayers on Metal Surfaces: Factor Analysis of Mixed Monolayers. *Anal. Chem.* **2019**, *91* (2), 1269−1276.
(57) Shen, Y. R. A few selected applications of surface nonlinear optical spectroscopy. *Proc. Natl. Acad. Sci. U. S. A.* **1996**, *93* (22), 12104−12111.
(58) Wenzl, I.; Yam, C. M.; Barriet, D.; Lee, T. R. Structure and wettability of methoxy-terminated self-assembled monolayers on gold. *Langmuir* **2003**, *19* (24), 10217−10224.
(59) Lee, S.; Puck, A.; Graupe, M.; Colorado, R.; Shon, Y. S.; Lee, T. R.; Perry, S. S. Structure, wettability, and frictional properties of phenyl-terminated self-assembled monolayers on gold. *Langmuir* **2001**, *17* (23), 7364−7370.
(60) Durig, J. R.; Yu, Z.; Guirgis, G. A. Conformational stability, barriers to internal rotation, vibrational assignment, and ab initio calculations of 2,2-difluorobutane. *J. Mol. Struct.* **1999**, *509* (1−3), 115−135.
(61) Durig, J. R.; Guirgis, G. A.; Li, Y. S. Microwave, Raman, and Far Infrared-Spectra, Barrier to Internal-Rotation, and Dipole-Moment of 2,2-Difluoropropane. *J. Chem. Phys.* **1981**, *74* (11), 5946−5953.
(62) McNaughton, D.; Evans, C. High-resolution FTIR spectrum of jet-cooled CH3CHF2. *J. Phys. Chem.* **1996**, *100* (21), 8660−8664.
(63) Nanaie, H.; Guirgis, G. A.; Durig, J. R. Torsional Spectra of Molecules with 2 C-3v Rotors 0.25. Rotational and Vibrational-Spectra, R(0) Structure, Barriers to Internal-Rotation and Ab-Initio Calculations for 2,2-Difluoropropane. *Spectrochim Acta A* **1993**, *49* (13−14), 2039−2056.
(64) Li, Y. S.; Cox, F. O.; Durig, J. R. Low-Resolution Microwave, Infrared, and Raman-Spectra, Conformational Stability, and Vibrational Assignment of 2,2,2-Trifluoroethyl Methyl-Ether. *J. Phys. Chem.* **1987**, *91* (6), 1334−1344.
(65) Guyot-Sionnest, P.; Hunt, J. H.; Shen, Y. R. Sum-frequency vibrational spectroscopy of a Langmuir film: Study of molecular orientation of a two-dimensional system. *Phys. Rev. Lett.* **1987**, *59* (14), 1597−1600.
(66) Bain, C. D.; Davies, P. B.; Ward, R. N. In-Situ Sum-Frequency Spectroscopy of Sodium Dodecyl-Sulfate and Dodecanol Coadsorbed at a Hydrophobic Surface. *Langmuir* **1994**, *10* (7), 2060−2063.

https://dx.doi.org/10.1021/acs.jpcc.0c02038
J. Phys. Chem. C 2020, 124, 16908−16917